

Volume Conduction in an Anatomically Based Surface EMG Model

Madeleine M. Lowery*, *Member, IEEE*, Nikolay S. Stoykov, *Member, IEEE*, Julius P. A. Dewald, and Todd A. Kuiken, *Member, IEEE*

Abstract—A finite-element model to simulate surface electromyography (EMG) in a realistic human upper arm is presented. The model is used to explore the effect of limb geometry on surface-detected muscle fiber action potentials. The model was based on magnetic resonance images of the subject's upper arm and includes both resistive and capacitive material properties. To validate the model geometry, experimental and simulated potentials were compared at different electrode sites during the application of a subthreshold sinusoidal current source to the skin surface. Of the material properties examined, the closest approximation to the experimental data yielded a mean root-mean-square (rms) error of the normalized surface potential of 18% or 27%, depending on the site of the applied source. Surface-detected action potentials simulated using the realistic volume conductor model and an idealized cylindrical model based on the same limb geometry were then compared. Variation in the simulated limb geometry had a considerable effect on action potential shape. However, the rate of decay of the action potential amplitude with increasing distance from the fiber was similar in both models. Inclusion of capacitive material properties resulted in temporal low-pass filtering of the surface action potentials. This effect was most pronounced in the end-effect components of action potentials detected at locations far from the active fiber. It is concluded that accurate modeling of the limb geometry, asymmetry, tissue capacitance and fiber curvature is important when the specific action potential shapes are of interest. However, if the objective is to examine more qualitative features of the surface EMG signal, then an idealized volume conductor model with appropriate tissue thicknesses provides a close approximation.

Index Terms—Capacitance, EMG, finite-element, geometry, MRI.

Manuscript received June 20, 2003; revised May 9, 2004. Asterisk indicates corresponding author.

*M. M. Lowery is with the Sensory Motor Performance Program Laboratory, Research Department, Rehabilitation Institute of Chicago, Chicago, IL 60611-4496 USA and also with the Department of Physical Medicine and Rehabilitation, Northwestern University, Evanston, IL 60611 USA (e-mail: m-lowery@northwestern.edu).

N. S. Stoykov is with the Sensory Motor Performance Program Laboratory, Rehabilitation Institute of Chicago, IL 60611 USA and also with the Department of Physical Medicine and Rehabilitation, Northwestern University, Chicago, IL 60611 USA (e-mail: n-stoykov@northwestern.edu).

J. P. A. Dewald is with the Sensory Motor Performance Program Laboratory, Rehabilitation Institute of Chicago, IL 60611 USA and also with the Departments of Physical Therapy & Human Movement Science, Northwestern University, IL 60611 USA (e-mail: j-dewald@northwestern.edu).

T. A. Kuiken is with the Sensory Motor Performance Program Laboratory, Rehabilitation Institute of Chicago, IL 60611 USA and with the Departments of Physical Medicine and Rehabilitation and Department of Electrical and Computer Engineering, Northwestern University, IL 60611 USA (e-mail: tkuiken@rehabchicago.org).

Digital Object Identifier 10.1109/TBME.2004.836494

I. INTRODUCTION

MATHEMATICAL modeling of the surface electromyographic (EMG) signal has become a valuable tool with which to explore appropriate methods of uncovering underlying motoneuron and muscle activation patterns. Understanding how different physiological and physical factors alter the signal detected at the skin surface is central to this aim. Although the influence of muscle fiber location, electrode configuration, tissue conductivity and muscle anisotropy have been widely examined [1]–[4], the effect of limb geometry on the surface EMG signal has not yet been explored. The majority of EMG models which have been presented are based on solutions for muscle fibers located in homogenous volume conductors of infinite extent [5]–[8]. While computationally efficient, particularly in the simulation of large numbers of motor units [9]–[11], infinite volume conductor models do not allow variations in tissue properties or inhomogeneous structures to be included. To incorporate the effect of skin and fat tissue, volume conductor models based on concentric cylinders or uniform layers have been developed [2], [12], [13]. Muscle fiber action potentials in realistic limb geometries have not yet been simulated, however, largely due to the limited volume conductor shapes for which analytical solutions are readily available. Associated with variations in the limb anatomy, is the path that is traversed by the muscle fibers. Using model simulation, it has been illustrated that fiber curvature can alter the shape of nerve and muscle fiber action potentials recorded in finite and infinite volume conductor models, respectively [14], [15]. The majority of EMG simulation models to date, however, have assumed the muscle fibers to be straight.

To address more complex limb anatomies, numerical techniques such as the boundary element, finite difference or finite-element methods must be employed. Numerical methods have been widely applied in electrocardiography [16] and electroencephalography [17]. However, with few exceptions, [18]–[20], their application to volume conduction of EMG signals has been limited to date. Recent numerical simulations using a finite-element model of an idealized cylindrical limb have yielded results which are consistent with previous analytical studies, and have been used to examine the effect of bone, fat thickness and frequency dispersion in the muscle conductivity and permittivity [21], [22]. In this paper, the finite-element EMG model presented in [21] and [22] is extended to simulate surface EMG signals in an anatomically accurate, volume conductor model of the human upper arm. The finite-element approach enables models that reflect the complex anatomies of human limbs, including asymmetrical geometries and fibers of arbitrary orientation, to be developed. The model presented includes bone, muscle, fat,

and skin tissue based on magnetic resonance (MR) images of the upper arm of a single male subject. Although it is generally assumed that for EMG applications muscle, fat, and skin tissues behave as if they are purely resistive, experimental [23] and recent simulation results [21] suggest that capacitive effects may be significant in the frequency range of surface EMG signals. Both the conductivity and permittivity of all tissues are, therefore, included.

One of the most challenging areas in the development of detailed volume conductor models is validation of the simulation results. When considering physiological current sources, it is particularly difficult to localize the origin of the excitation, as there is currently no *in vivo* method to reliably determine the number of muscle fibers in a particular motor unit and the shape and size of the territory through which they are distributed. One of the earliest studies to directly compare experimentally recorded and simulated motor unit action potentials was presented by Griep *et al.*, [7]. In their study, motor unit action potentials recorded at the surface of the extensor digitorum longus muscle in rat were compared with simulated action potentials where fiber and motor end-plate locations were obtained from the experimental preparation. An alternative approach was presented by Roeleveld *et al.*, [12] who compared surface motor unit action potentials from the human biceps muscle with simulated action potentials generated by muscle fibers located at the electrical center of the experimentally recorded motor units. To avoid the complexities associated with localizing the motor unit action potential and its constituent fibers, in this study the voltage distribution around the surface of the limb was recorded during the application of a current source at an intensity below the threshold required for stimulation of the underlying muscle fibers. The recorded surface potential distribution is compared with data simulated using the anatomically based model for the same subject. The subject-specific model is then used to explore how limb geometry may affect action potentials recorded at the skin surface. Action potentials are simulated for both curved and straight muscle fibers located in the subject specific volume conductor. The effects of tissue capacitance and of local inhomogeneities due to subcutaneous blood vessels on the surface action potentials are also examined.

II. METHODS

A. Experimental Methods

A single healthy male subject (46 years old, height 1.92 m, weight 97 kg) participated in the experiments. A guide-line was drawn around the circumference of the subject's right arm, halfway between the medial condyle and the acromium. The subject's skin was prepared by gentle abrasion and cleansing with alcohol. Sixteen active, single differential bipolar silver bar electrodes (Delsys Inc., Boston, MA) were then placed around the arm, 50 mm below the guide-line. Each electrode consisted of two 10 mm \times 1 mm silver bars, separated by an inter-electrode distance of 10 mm. The bipolar electrodes were placed side by side, with a distance of 12 mm between the bars of adjacent electrode pairs and the long axis of each bar aligned perpendicular to the muscle fiber direction. The electrode located above the brachial artery was labeled electrode

4 and the electrodes were numbered in ascending order in the lateral direction. Two pregelled circular excitation electrodes, 10-mm diameter, were placed 60 mm apart in the direction of the muscle fibers, one on either side of recording electrode 4. A second pair of excitation electrodes was placed one on either side of electrode 7.

The subject was seated in an adjustable chair with the right arm supported. The shoulder was positioned at 60° of abduction and 45° of flexion, the elbow was flexed at 90° with the forearm in a mid pronated-supinated position. A 1 mA, 100 Hz, constant current source was applied to the skin surface at the excitation electrodes located about recording electrode 4. The intensity of the applied source was below the threshold for excitation of the underlying muscle fibers. The voltage at each electrode was recorded during ten consecutive 2-s epochs. The recordings were then repeated with the excitation electrodes placed on either side of electrode 7. The data were recorded at a sampling frequency of 2 kHz, and bandpass filtered between 10 and 450 Hz. The experimental recordings were repeated on three separate days.

B. Finite-Element Models

The experimentally recorded surface potentials were compared with data simulated using two different finite-element models—an anatomically based model, derived from MR images of the upper arm of the same subject, and an idealized cylindrical arm model. EMG signals at the skin surface due to single muscle fibers in the subject-specific and idealized finite-element models were then compared. Consistent with previous EMG models, wave propagation and inductive effects were assumed to be negligible [24]. However, unlike previous EMG models which assume the biological tissues to be purely resistive in the frequency range of interest, capacitive effects were included in the finite-element simulations.

The electric field, \vec{E} , in the volume conductor is described by Maxwell's equation derived from Ampere's Law in point form

$$\nabla \cdot \left(\epsilon \frac{\partial \vec{E}}{\partial t} + \sigma \vec{E} \right) = 0 \quad (1)$$

where σ is the conductivity and ϵ is the permittivity of the medium. \vec{E} is assumed to be a gradient field, i.e., $\vec{E} = -\nabla\phi$, where ϕ is the electric scalar potential.

The finite-element model meshes were generated and the potential throughout the model solved using the EMAS software package (EMAS 4.1, Ansoft Corp., Pittsburgh, PA), using two-dimensional (2-D) elements along the surface of the skin and three-dimensional (3-D), linear, tetrahedral elements throughout the remainder of the model. To verify that a 3-D layer of skin could be approximated by a layer of 2-D elements along the surface of the fat tissue, the potential at each electrode due to a 1-mA surface excitation was compared when the 1.3-mm layer of skin tissue was modeled using 3-D elements and when the tissue was simulated using 2-D elements along the surface of the fat tissue. The distance between adjacent nodes of the mesh varied from 0.1 mm, along the muscle fiber, to 8 mm deeper within the volume conductor. Care was taken

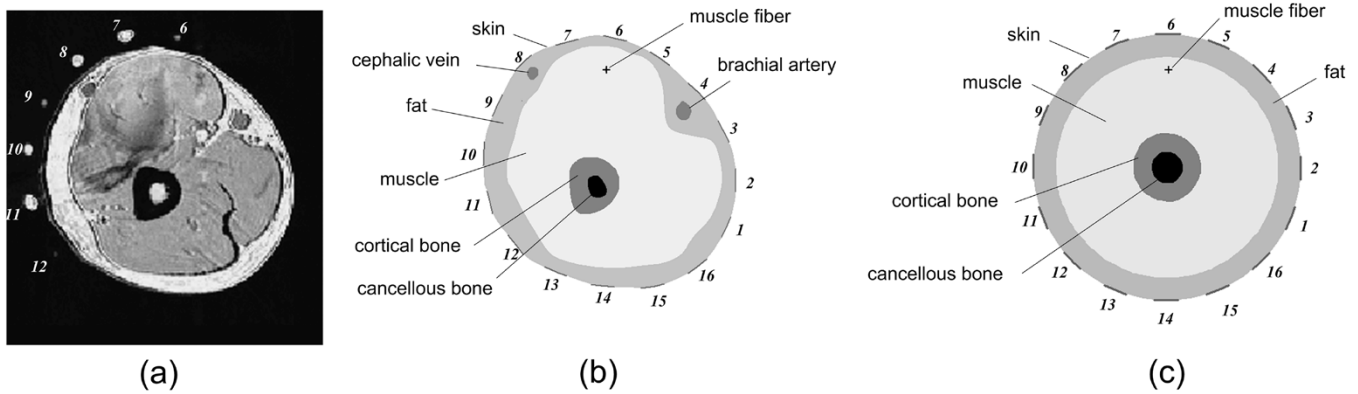


Fig. 1. Transverse cross section of subject's right arm (a) MR image mid-way between the bipolar surface electrodes. The location of the electrodes are visible as light colored markers. Markers not visible in this slice were visible in either the previous or subsequent MR image. (b) Cross section of subject-specific model at the same location. (c) Cross section of idealized cylindrical model based on image shown in (a).

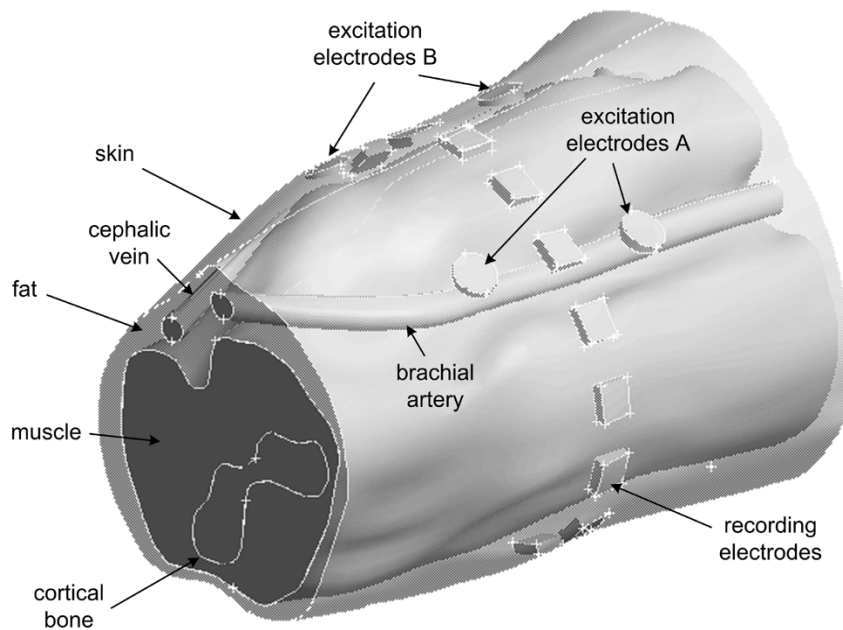


Fig. 2. Geometry of anatomically based volume conductor model illustrating the tissue geometries and surface electrodes.

to confirm that further reducing the size of the mesh elements did not alter the voltage at the recording electrodes.

1) *Subject Specific Model:* A series of MR images of the right upper arm of the same subject that took part in the experimental recordings was acquired. Rectangular plastic markers, equal in dimension to the electrodes used in the experimental study, were placed around the surface of the subject's right arm at locations corresponding to the electrode location in the experimental protocol. Oil capsules were placed at the center of each electrode marker to ensure visibility in the MR images. The subject was positioned lying down with the right arm above the head, inside a limb coil, parallel to the trunk. Transverse images of the upper arm were acquired with an in-plane resolution of 256×256 pixels, 3-mm slice thickness and pixel size of 0.8 mm^2 using a 1.5 T Siemens scanner, Fig. 1(a).

The outlines of the fat, muscle, cortical bone and cancellous bone tissues were digitized from a series of transverse images, 30 mm apart. The data were imported into a commercially available finite-element software package (EMAS 4.1,

Ansoft Corp., Pittsburgh, PA). A spline was fitted through the data points corresponding to the outline of each tissue, yielding a series of curves along the surface of the fat, muscle, cortical bone and cancellous bone tissues at 30-mm intervals along the arm, Fig. 1(b). A 3-D solid was then created by generating a skin function over the outline of each tissue, interpolating the surface geometry between splines, and creating separate regions of the volume conductor for each tissue, Fig. 2. The total length of the volume conductor was 180 mm, centered 50 mm below the mid-point of a line connecting the leading edge of the acromion and the lateral condyle of the humerus.

Sixteen pairs of 10-mm-long bipolar silver bar electrodes, with an inter-electrode distance of 10 mm, were located around the surface of the model at the locations of the markers in the MR images. A 120-mm-long muscle fiber was simulated 14.5 mm below the surface of the volume conductor directly below electrode 6. The fiber was curved to follow the surface of the model, remaining at a constant depth at all points along the axial direction. A straight muscle fiber orientated parallel to the surface of

TABLE I
CONDUCTIVITY (σ) AND RELATIVE PERMITTIVITY (ϵ) OF MUSCLE, FAT AND SKIN TISSUE FOR THE ANATOMICAL VOLUME CONDUCTOR MODELS AND THE IDEALIZED MODEL. THE MEAN rms ERROR OF THE NORMALIZED PEAK-PEAK AMPLITUDE DURING THE APPLICATION OF A SUBTHRESHOLD SURFACE EXCITATION APPLIED ON EITHER SIDE OF ELECTRODES 4 AND 7 IS ALSO PRESENTED. ^aGABRIEL *et al.*, [27]; ^bFOSTER AND SCHWAN, [26]; ^cGIELEN *et al.*, [23]; ^dYAMAMOTO AND YAMAMOTO, [29] (GRANULAR TISSUE)

Model	Muscle <i>longitudinal direction</i>		Muscle <i>transverse direction</i>		Fat		Skin		Mean rms error	
	σ_l (S/m)	ϵ_l	σ_t (S/m)	ϵ_t	σ_f (S/m)	ϵ_f	σ_s (S/m)	ϵ_s	Excitation 4	Excitation 7
A	0.30 ^a	3x10 ^{7a}	0.20 ^a	1x10 ^{7a}	0.04 ^a	1.5x10 ^{5a}	4.3x10 ^{-4a}	4.5x10 ^{4a}	69.59%	134.48%
B	0.52 ^b	1.1x10 ^{6b}	0.076 ^b	3.2x10 ^{5b}	0.07 ^b	1.5x10 ^{5b}	4.3x10 ^{-4a}	4.5x10 ^{4a}	29.76%	28.95%
C	0.40 ^c	2x10 ^{7c}	0.09 ^c	4.4x10 ^{6c}	0.04 ^a	1.5x10 ^{5a}	4.3x10 ^{-4a}	4.5x10 ^{4a}	26.61%	18.00%
D	0.40 ^c	2x10 ^{7c}	0.09 ^c	4.4x10 ^{6c}	0.04 ^a	1.5x10 ^{5a}	2.2x10 ^{-2d}	4.0x10 ^{5d}	26.15%	20.40%
Idealized	0.40 ^c	2x10 ^{7c}	0.09 ^c	4.4x10 ^{6c}	0.04 ^a	1.5x10 ^{5a}	4.3x10 ^{-4a}	4.5x10 ^{4a}	31.5 %	29.2 %

the bone was also simulated at the same depth below electrode 6.

To compare data simulated using the subject-specific model directly with the experimental data, two pairs of 10-mm diameter, circular, excitation electrodes were simulated 60 mm apart along the longitudinal axis of the model. One pair of electrodes was centered on recording electrodes 4, the other pair on recording electrodes 7 as in the experimental protocol, Fig. 2(a).

2) *Idealized Cylindrical Limb Model*: The idealized cylindrical limb model was based on the cross-sectional MR image located at the center of the bipolar recording electrodes, Fig. 1(c). The model consisted of concentric layers of bone, muscle, fat, and skin as described in [22]. The diameter of each tissue was estimated by calculating the mean diameter of the tissue in the MR image. The total diameter of the idealized model was 108 mm, with a distance of 6 mm from the center of the model to the surface of the cancellous bone, 13.5 mm to the surface of the cortical bone, and 44.5 mm to the surface of the muscle tissue, yielding a fat thickness of 9.5 mm. Sixteen pairs of recording electrodes were equally spaced around the center of the model and a pair of excitation electrodes with a 60-mm interelectrode distance was centered about a pair of recording electrodes. A muscle fiber 120 mm in length was located 14.5 mm below the skin surface at electrode 6, as in the subject-specific model.

3) *Boundary Conditions*: At the boundary of the model, it was assumed that the normal component of the electric field is equal to zero. In previous finite-element EMG models, we have assumed the volume conductor to be of infinite length by applying boundary conditions based on the Bayliss-Turkel approximation [22] at either end of the model. To avoid the additional complexities associated with applying open boundary conditions on the subject specific geometry it was assumed here that the model was of finite length. In this case, current is no longer free to flow into the distal and proximal ends of the limb. The potential at the surface of the volume conductor was examined as the length of each model was progressively increased to confirm that the model was sufficiently long that the potential at the electrodes did not vary with the length of the volume conductor. The potential at the node farthest from the recording electrodes was set to equal zero.

4) *Material Properties*: There is considerable variability in the values of conductivity and relative permittivity that have been reported for biological tissues, particularly for skeletal

muscle and fat tissue. In the data reviewed by Geddes and Baker [25], conductivity values for muscle in the longitudinal direction vary between 0.093 S/m and 0.8 S/m at 100 Hz, with anisotropy values ranging from 1.8 to 14.4. Low frequency conductivity values for fat tissue similarly range from 0.02 S/m to 0.1 S/m [25], [26]. Because of the large spread of reported material properties, the experimental data were compared with data simulated using the anatomical model with several different combinations of muscle and fat dielectric properties reported in the literature [23]–[27]. The conductivity and relative permittivity values for each tissue were chosen at 100 Hz, in the region of the median frequency of typical surface EMG signals. Muscle tissue was assumed to be cylindrically anisotropic in both conductivity and permittivity, while bone, fat, and skin were assumed to be isotropic. The conductivity and permittivity values for muscle, fat, and skin tissue in each model are presented in Table I. Cortical and cancellous bone were assigned a conductivity of 0.02 S/m and 0.08 S/m and a relative permittivity of 6×10^3 and 2×10^4 , respectively [28]. The material properties for blood were selected for the conductivity, 0.66 S/m, and permittivity, 1.4×10^3 , of the artery and vein [28]. Skin was simulated as a homogeneous tissue although in reality it has a laminar structure, with most of the impedance due to the highly resistive stratum corneum, which becomes less resistive with increasing depth. Below the highly resistive barrier layer lies deeper granular tissue with material properties closer to those of muscle tissue [29]. The conductivity of wet skin used in Models A, B, and C lies between the reported for the different skin layers [27], while the more conductive tissue used in Model D has the material properties reported for the granular layer [29]. Material properties for the idealized model were the same as those used in anatomically based models, Table I.

5) *Muscle Fiber Action Potentials*: To simulate the surface-detected action potential, the voltage at the skin surface due to the propagation of a series of current sources along the muscle fiber was calculated at each time step, using the finite-element method. Action potential sources propagated along each fiber, in both directions away from the muscle fiber end-plate, with a conduction velocity of 4 m/s. The muscle fiber end-plate was located mid-way along the fiber, 20 mm from the center of the recording electrodes. The propagating current sources were obtained by discretizing the second derivative of the transmembrane action potential described analytically by

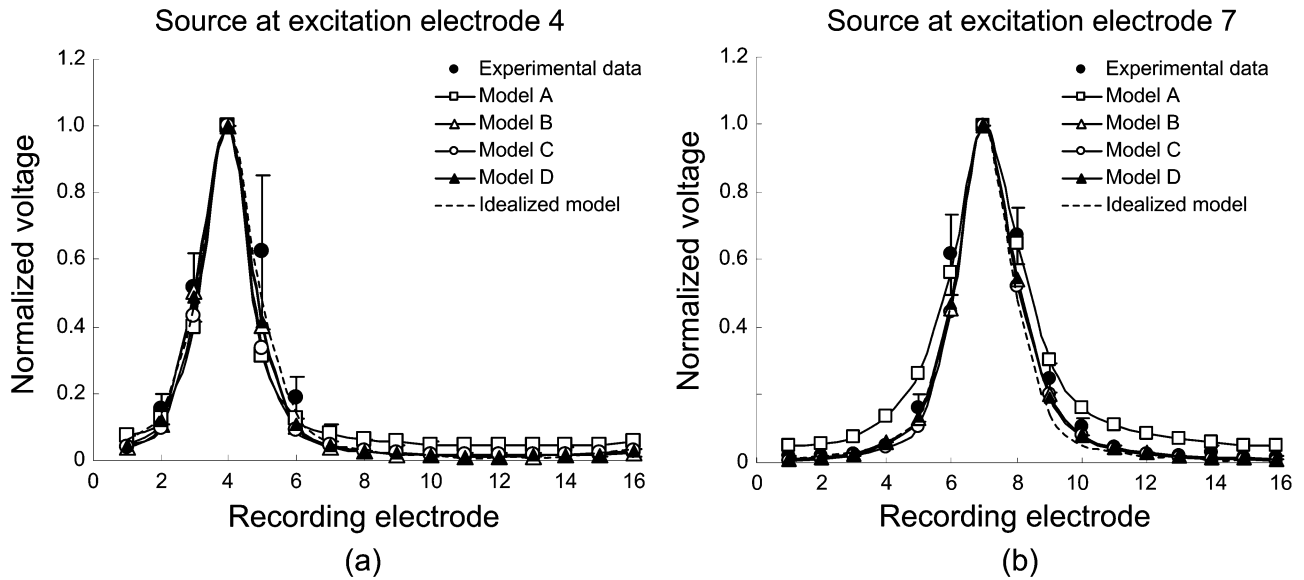


Fig. 3. Comparison of experimental and simulated surface potential for a subthreshold, sinusoidal excitation applied to the surface of the arm. All data have been normalized with respect to the maximum potential at the recording electrodes. Simulated data are presented for the anatomically based model using the material properties detailed in Table I, and for the idealized model using the material properties of Model C. (a) Excitation electrodes applied on either side of electrode 4. (b) Excitation electrodes applied on either side of electrode 7.

Rosenfalck [30], at 0.1-mm intervals between 0 and 38 mm, and scaling appropriately, [30]. Muscle fiber end-effects were incorporated by applying compensating currents equal in magnitude and opposite in sign to the integral of the applied current along the fiber, to the fiber end-plate at the generation of the action potentials and to the fiber terminations at the action potential extinction thus ensuring that the total current in the model was equal to zero at all times [2], [31]. The action potential simulations were conducted using dielectric properties of muscle reported by Gabriel *et al.*, [27], [32] (Model A) and by Gielen *et al.*, [23] (Model C).

C. Simulation Details

The finite-element method was used to calculate the potential in the anatomical and idealized volume conductor models due to an applied excitation identical to that used in the experimental methods. The voltage around the surface of each model was examined as a 100-Hz sinusoidal excitation, peak-peak amplitude 1 mA, was applied to each set of excitation electrodes in succession. Surface-detected action potentials from the subject-specific anatomical model, with straight and curved muscle fibers, and the idealized cylindrical model were then simulated. The simulations were repeated for an effectively resistive anatomical model with the relative permittivity of all tissues set equal to one. The brachial artery was included in the model of the propagating action potential, while both the brachial artery and the cephalic vein were included in the model of the applied surface excitation, Fig. 1(b). To examine the influence of the blood vessels on the surface potential, the potential at each electrode was examined when the vein and artery were removed from the subject specific model with both the surface excitation and muscle fiber action potential source.

The potential at each electrode was calculated at 0.25-ms intervals using the EMAS (Ansoft Corp., Pittsburgh, PA) time domain solver. The simulations were executed on a Dell Dimen-

sion 8100 PC with a 1.5-GHz Intel Pentium 4 processor and 512 MB RAM. Typical computation time for the subject-specific model with a propagating action potential source and a total of 549 779 elements was 50 min.

III. RESULTS

A. Surface Excitation

In Fig. 3, the mean and standard deviation of the peak-peak voltage recorded at each electrode during the application of the subthreshold surface excitation is compared with data simulated using the finite-element model. Data is presented for the anatomically based model using different muscle and fat dielectric properties, models A, B, C, and D, Table I, and for the idealized cylindrical model using the material properties for model C. All of the data have been normalized with respect to the voltage recorded at the surface electrode closest to the source. With the excitation applied on either side of electrodes 4, the maximum voltage at the recording electrodes before normalization was 27.22 mV (± 2.2) (experimental data), 42.8 mV (model A), 35.2 mV (model B), 47.2 mV (model C), 51.8 (model D) and 39.1 mV (idealized cylindrical model). With the excitation applied on either side of electrode 7, the maximum voltage was 43.1 mV (± 8.7) (experimental data), 25.7 mV (model A), 34.2 mV (model B), 36.7 mV (model C), 44.1 (model D) and 39.1 mV (idealized cylindrical model). The mean root-mean-square (rms) errors between the simulated and experimental peak-peak voltage at the recording electrodes in the various models are compared in Table I.

B. Simulated Single Fiber Action Potential

Simulated surface action potentials from a 14.5-mm deep muscle fiber are presented in Fig. 4. Action potentials were simulated for a curved and straight muscle fiber in the subject-specific model, and for a straight fiber in the idealized

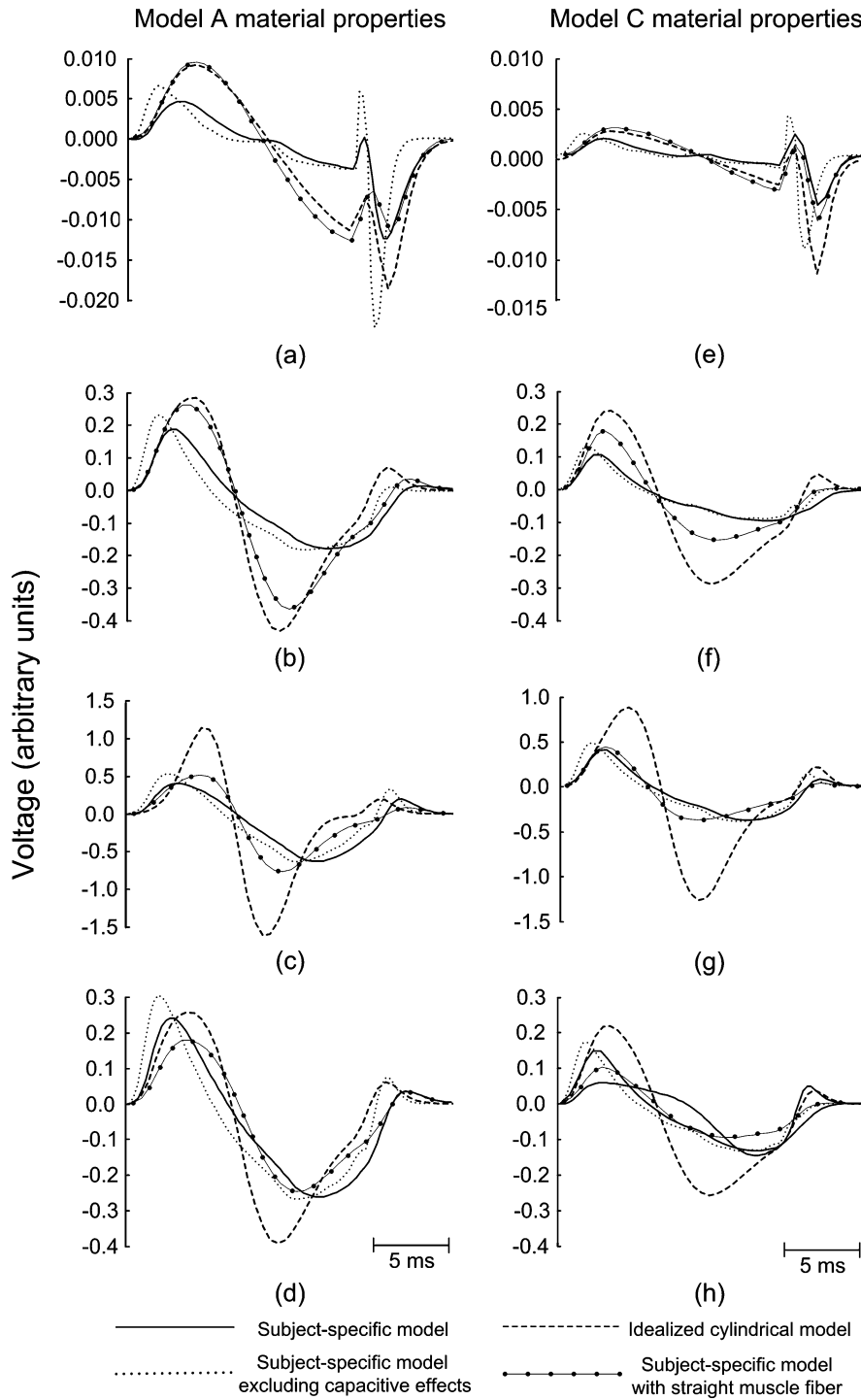


Fig. 4. Simulated surface action potentials for a fiber located 14.5 mm below the skin surface beneath electrode 6. Action potentials are presented at different electrode locations for the subject specific anatomical model with both resistive and capacitive material properties (solid line), purely resistive material properties (dotted line), a straight muscle fiber (dot-dashed line) and for the equivalent idealized cylindrical model (dashed line). The action potentials in (a)–(d) were simulated using the material properties of Model A, those in (e)–(h) using the material properties of Model C. (a) Electrode 2, (b) Electrode 5, (c) Electrode 6, (d) Electrode 7, (e) Electrode 2, (f) Electrode 5, (g) Electrode 6, (h) Electrode 7.

cylindrical model. Action potentials from the curved muscle fiber were also examined when capacitive effects were removed from the model. Data is presented for two combinations of material properties, Models A and C, Table I. The normalized rms values of the surface action potentials are presented in Fig. 5(a) and the median frequencies of the power spectra of the action potential waveforms in Fig. 5(b). Variations in the

volume conductor geometry and the curvature of the fiber yielded substantial differences in the shape and amplitude of the simulated surface action potentials, Fig. 4. This is also reflected in the median frequencies of the surface potentials, Fig. 5(b). However, the rate of decay of the action potentials simulated with the idealized and subject specific models were very similar Fig. 5(a).

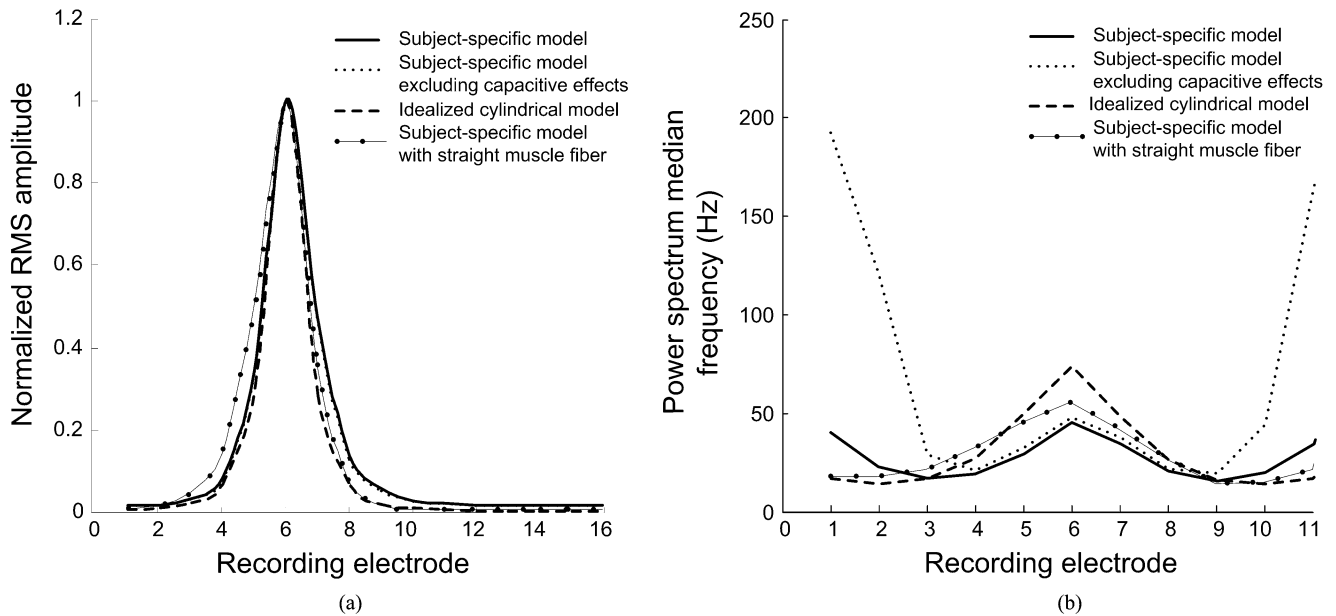


Fig. 5. (a) Normalized rms amplitude of the surface action potential at different electrode locations from a 14.5-mm deep muscle fiber in the anatomical model, with both resistive and capacitive material properties (solid line), purely resistive material properties (dotted line), a straight muscle fiber (dot-dashed line) and in the equivalent idealized cylindrical model. (b) Median frequency of the surface action potentials at different electrode locations. Material properties are those described for Model A, Table I.

Inclusion of capacitive tissue properties produced a slight phase shift in the surface action potentials with respect to the purely resistive model and a reduction in the amplitude of the waveform start-up and end-effects. At recording electrode sites located closest to the muscle fiber there was little variation between action potentials simulated using a purely resistive model and those simulated with both resistive and capacitive effects Fig. 4(c) and (g), Fig. 5(b). However, at electrode sites farther from the active fiber, differences due to the capacitance effects became more pronounced, Fig. 4(a) and (e). For example, in Model C, removing the tissue capacitance caused a 4.1% increase in the rms value of the action potential recorded directly above the fiber at electrode 6 and a 47.5% increase in the rms value at electrode 2, Fig. 4(e) and (g).

C. Effect of Blood Vessels

The potential at each electrode was examined when the blood vessels were removed from the model and replaced with fat tissue. Removing the blood vessels caused the potential at all electrode locations to increase. For example, using the material properties described for Model A, with the surface excitation applied at electrode 4, the greatest increase in voltage when the blood vessels were removed occurred at recording electrode 4 (28.15%), located directly above the brachial artery. With the excitation applied on either side of recording electrode 7, the greatest difference was 12.33% and occurred at recording electrode 8, located directly above the cephalic vein. For simulated action potentials, the greatest change in potential also occurred at the electrode above the brachial artery, electrode 4. Replacing the blood vessel with fat tissue caused a 26.16% increase in the rms value of the surface action potential at this electrode. Similar results were observed with all other combinations of material properties.

IV. DISCUSSION

A new model to simulate surface EMG in an anatomically based volume conductor is presented. The anatomically based model represents a new approach in surface EMG simulation and allows the incorporation of features that cannot be included using traditional analytical methods. These include conducting electrodes, uneven surfaces and asymmetrical tissue geometries. Previous surface EMG simulation studies model the limb as an infinite, semi-infinite or symmetrical cylindrical volume conductor, and assume capacitive effects to be negligible at the frequencies of interest. It is also generally assumed that the muscle fibers run in a straight line, either parallel to, or inclined with respect to the skin surface. In comparison with analytical models, however, the complex finite-element models can be relatively time-consuming to develop and computationally demanding to execute. In order to reduce the computational burden, the 3-D skin tissue was modeled using 2-D finite elements. The models were also assumed to be of finite length, with ground located at the node farthest from the recording electrodes, rather than incorporate absorbing boundary conditions as in previous simulations [22]. Both of these simplifications considerably eased the generation of the finite-element mesh and reduced the computation time, without altering the potential distribution at the recording electrodes.

Although the conductivity and permittivity of biological tissues are well known to vary with frequency [26], classical EMG models assume that at the frequencies of interest biological tissues behave as if they are purely conductive materials, with constant conductivity. Consistent with these models, it was assumed that the material properties of all tissues remain constant across all frequencies. Conductivity and permittivity values for the simulations were chosen from values reported at a single frequency, 100 Hz, which lies close to the median frequency of

typical surface EMG signals and experimental measurements were conducted for a surface excitation at 100 Hz.

The rate of decay of a simulated subthreshold, surface excitation in both the subject-specific and idealized models was similar to that observed experimentally, Fig. 3. Of the limited combinations of material properties that were simulated, the model using muscle material properties reported by Gielen *et al.*, [23] provided the closest agreement between the simulated and experimental data, with a mean rms error of 26.6% (excitation at electrode 4) or 18% (excitation at electrode 7). Given the large number of variables in the model, it is likely that there are many different combinations of conductivity and permittivity that would yield similar results for a single geometry. There is considerable variability in the values of conductivity and permittivity that have been reported for skeletal muscle, fat, and skin tissue, and in reported muscle anisotropy values. The muscle tissue was assumed to be a cylindrically anisotropic, homogenous tissue, which assumes straight parallel muscle fibers. In the case of curved muscle fibers, however, the principal directions of the conductivity tensor vary within the muscle volume. While care was taken to ensure that the electrodes were placed at the same location in both the experiments and model simulations, it is possible that there were small variations in the electrode location between experiments or that the subcutaneous tissues may have moved relative to the skin surface. Due to the shape of the MR coil, it was not possible to place the subject's arm in exactly the same position as in the experimental protocol, which may result in slight differences in the limb anatomy between the two situations. Each of these factors could further contribute to the differences observed between the experimental and simulated voltages.

To examine how limb geometry can influence muscle fiber action potentials detected at the skin surface, action potentials simulated using the anatomically correct volume conductor model and the idealized cylindrical model were compared. The rate of decay of the action potential amplitude around the limb was similar in both models, Fig. 5(a). However, the shapes of the individual action potentials varied considerably, Figs. 4 and 5(b). The greatest variations in action potential shape were observed at electrode locations farthest from the active fiber, where the amplitude of the detected signal and its contribution to the surface EMG signal are small. At electrode locations closer to the fiber where the contribution from the muscle fiber is greatest, for example at electrodes 4 to 9, variations between simulated action potentials in the different models were considerably less.

Curvature of the muscle fiber was also observed to influence the shape of the surface-detected action potentials. At electrode locations close to the source, action potentials from the straight and curved muscle fibers in the subject-specific model were quite similar. However, as the distance between the fiber and the detection electrode increased, the action potentials from the straight fiber were closer in shape to the idealized cylindrical limb model than to a curved fiber in the subject-specific model. From the simulation results, it is suggested that the specific geometry of the limb is an important factor if details of individual action potential shapes are of interest. However, if the main parameters of interest are more qualitative features of the EMG signal, such as the approximate rate of decay of the EMG amplitude or factors related to the motor unit firing patterns, then an idealized cylindrical limb model with

appropriate thicknesses of fat tissue provides a close approximation to the anatomically correct model.

Inclusion of capacitive effects in the model resulted in a phase shift of the detected action potentials with respect to the purely resistive model and a reduction in the amplitude of the muscle fiber end-effect components, Fig. 4. The attenuation of the fiber end-effects was most pronounced at electrode locations farthest from the active fiber, where the relative contribution of the end-effect component is greatest, Fig. 4(a) and (e). Introducing the tissue capacitance caused the volume conductor to behave like a temporal low-pass filter. This temporal low-pass filtering effect is distinct from the spatial filtering of the propagating action potential that is also observed in purely resistive volume conductor models. In the examples presented, temporal filtering caused an attenuation of the muscle fiber end-effects, which tend to have a higher frequency content than the propagating part of the waveform and whose relative contribution to the surface action potential is greatest at large distances from the fiber [33]. The median frequencies of surface action potentials at electrodes sites farthest from the fiber, therefore, decreased when capacitive tissue properties were included, while the median frequencies of action potentials detected closer to the fiber remained relatively unchanged, Fig. 5(b).

For the dielectric properties of Models A and C, based on the measured muscle properties reported by Gabriel *et al.*, [27] and Gielen *et al.* [23], respectively, the tissue capacitive effects had a noticeable effect on the surface action potential waveforms. With other combinations of conductivity and relative permittivity, however, capacitive effects will be less significant or negligible [24]. Furthermore, dispersion in conductivity and permittivity has not been included in the present model. Previous simulations using a homogeneous finite-element muscle model have illustrated that neglecting the frequency-dependent, or dispersive, nature of muscle permittivity can cause capacitive effects to be overestimated in the simulation of single fiber action potentials [21]. To fully assess the contribution of capacitive currents to the surface EMG signal, dispersion in the material properties of each tissue should be incorporated.

Finally, the presence of highly conductive subcutaneous blood vessels was observed to alter the potential distribution along the surface of the model. The most pronounced change occurred at the recording electrodes directly above the vessel. Including a blood vessel, either the brachial artery or the cephalic vein, below the skin surface had a shunting effect, causing the potential at the electrode located directly above it to decrease. Rutten *et al.*, [20], have shown similar changes, either an increase or a decrease in the potential recorded in the vicinity of a blood vessel located at the center of a finite volume muscle model, depending on the observation point.

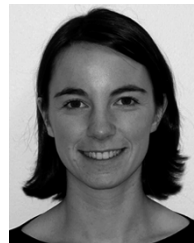
V. CONCLUSION

A new model of the surface EMG signal based on a realistic arm anatomy has been presented. The model includes both resistive and capacitive material properties. Comparison of experimental and simulated data for an applied subthreshold surface excitation confirmed that the finite-element model yielded a close approximation of the rate of decay of the applied surface

excitation around the upper arm. For simulated surface-detected muscle fiber action potentials, the specific geometry of the limb caused substantial variations in the shapes of the surface potentials. An idealized cylindrical volume conductor model with appropriate subcutaneous layers, however, provided a close approximation to the rate of decay of the surface action potential amplitude. Inclusion of tissue capacitance resulted in a temporal low-pass filtering of the surface action potentials which was most pronounced in the end-effects of action potentials detected at locations far from the source, and caused a slight reduction in the amplitude and frequency content of the signal. It is concluded that accurate modeling of limb geometry, asymmetry, tissue capacitance and fiber curvature is important when the specific shapes of the surface potentials are of interest.

REFERENCES

- [1] A. J. Fuglevand, D. A. Winter, A. E. Patla, and D. Stashuk, "Detection of motor unit action-potentials with surface electrodes—Influence of electrode size and spacing," *Biol. Cybern.*, vol. 67, pp. 143–153, 1992.
- [2] T. Gootzen, D. F. Stegeman, and A. Van Oosterom, "Finite limb dimensions and finite muscle length in a model for the generation of electromyographic signals," *Electroencephalogr. Clin. Neurophysiol.*, vol. 81, pp. 152–162, 1991.
- [3] D. Farina, C. Cescon, and R. Merletti, "Influence of anatomical, physical, and detection-system parameters on surface EMG," *Biol. Cybern.*, vol. 86, pp. 445–456, 2002.
- [4] G. V. Dimitrov, C. Disselhorst-Klug, N. A. Dimitrova, E. Schulte, and G. Rau, "Simulation analysis of the ability of different types of multi-electrodes to increase selectivity of detection and to reduce cross-talk," *J. Electromyogr. Kinesiol.*, vol. 13, pp. 125–138, 2003.
- [5] L. H. Lindstrom and R. I. Magnusson, "Interpretation of myoelectric power spectra—Model and its applications," *Proc. IEEE*, vol. 65, pp. 653–662, 1977.
- [6] D. C. Boyd, P. D. Lawrence, and P. J. Bratty, "On modeling the single motor unit action potential," *IEEE Trans. Biomed. Eng.*, vol. BME-25, pp. 236–43, 1978.
- [7] P. A. M. Griep, F. L. H. Gielen, H. B. K. Boom, K. L. Boon, L. L. W. Hoogstraten, C. W. Pool, and W. Wallinga-dejonge, "Calculation and registration of the same motor unit action-potential," *Electroencephalogr. Clin. Neurophysiol.*, vol. 53, pp. 388–404, 1982.
- [8] G. V. Dimitrov and N. A. Dimitrova, "Precise and fast calculation of the motor unit potentials detected by a point and rectangular plate electrode," *Med. Eng. Phys.*, vol. 20, pp. 374–81, 1998.
- [9] R. Merletti, L. Lo Conte, E. Avignone, and P. Guglielminotti, "Modeling of surface myoelectric signals—Part I: Model implementation," *IEEE Trans. Biomed. Eng.*, vol. 46, pp. 810–820, July 1999.
- [10] M. M. Lowery, C. L. Vaughan, P. J. Nolan, and M. J. O'Malley, "Spectral compression of the electromyographic signal due to decreasing muscle fiber conduction velocity," *IEEE Trans. Rehab. Eng.*, vol. 8, pp. 353–361, Sept. 2000.
- [11] J. Duchene and J. Y. Hogrel, "A model of EMG generation," *IEEE Trans. Biomed. Eng.*, vol. 47, pp. 192–201, Feb. 2000.
- [12] K. Roelleveld, J. H. Blok, D. F. Stegeman, and A. vanOosterom, "Volume conduction models for surface EMG; Confrontation with measurements," *J. Electromyogr. Kinesiol.*, vol. 7, pp. 221–232, 1997.
- [13] D. Farina and R. Merletti, "A novel approach for precise simulation of the EMG signal detected by surface electrodes," *IEEE Trans. Biomed. Eng.*, vol. 48, pp. 637–646, June 2001.
- [14] G. V. Dimitrov and N. A. Dimitrova, "Modeling of the extracellular potentials generated by curved fibers in a volume conductor," *Electromyogr. Clin. Neurophysiol.*, vol. 20, pp. 27–40, 1980.
- [15] S. Xiao, K. C. McGill, and V. R. Hentz, "Action potentials of curved nerves in finite limbs," *IEEE Trans. Biomed. Eng.*, vol. 42, pp. 599–607, June 1995.
- [16] A. van Oosterom and G. J. Huiskamp, "The effect of torso inhomogeneities on body surface potentials quantified using "tailored" geometry," *J. Electrocardiol.*, vol. 22, pp. 53–72, 1989.
- [17] J. Le and A. Gevins, "Method to reduce blur distortion from EEG's using a realistic head model," *IEEE Trans. Biomed. Eng.*, vol. 40, pp. 517–528, June 1993.
- [18] J. Schneider, J. Silny, and G. Rau, "Influence of tissue inhomogeneities on noninvasive muscle-fiber conduction-velocity measurements—investigated by physical and numerical modeling," *IEEE Trans. Biomed. Eng.*, vol. 38, pp. 851–860, Sept. 1991.
- [19] S. M. Wood, J. A. Jarratt, A. T. Barker, and B. H. Brown, "Surface electromyography using electrode arrays: A study of motor neuron disease," *Muscle Nerve*, vol. 24, pp. 223–230, 2001.
- [20] W. L. C. Rutten, B. K. van Veen, S. H. Stroeve, H. B. K. Boom, and W. Wallinga, "Influence of inhomogeneities in muscle tissue on single-fiber action potentials: A model study," *Med. Biol. Eng. Comput.*, vol. 35, pp. 91–95, 1997.
- [21] N. S. Stoykov, M. M. Lowery, A. Taflove, and T. A. Kuiken, "Frequency- and time-domain FEM models of EMG: Capacitive effects and aspects of dispersion," *IEEE Trans. Biomed. Eng.*, vol. 49, pp. 763–772, Aug., 2002.
- [22] M. M. Lowery, N. S. Stoykov, A. Taflove, and T. A. Kuiken, "A multiple-layer finite-element model of the surface EMG signal," *IEEE Trans. Biomed. Eng.*, vol. 49, pp. 446–454, May 2002.
- [23] F. L. H. Gielen, W. Wallinga-de Jonge, and K. L. Boon, "Electrical-conductivity of skeletal-muscle tissue-experimental results from different muscles in vivo," *Med. Biol. Eng. Comput.*, vol. 22, pp. 569–577, 1984.
- [24] R. Plonsey and D. B. Heppner, "Considerations of quasistationarity in electrophysiological systems," *Bull. Math. Biophys.*, vol. 29, pp. 657–664, 1967.
- [25] L. A. Geddes and L. E. Baker, "Specific resistance of biological material—A compendium of data for biomedical engineer and physiologist," *Med. Biol. Eng.*, vol. 5, pp. 271–293, 1967.
- [26] K. R. Foster and H. P. Schwan, "Dielectric properties of tissues and biological materials: A critical review," *Crit. Rev. Biomed. Eng.*, vol. 17, pp. 25–104, 1989.
- [27] S. Gabriel, R. W. Lau, and C. Gabriel, "The dielectric properties of biological tissues. 2. Measurements in the frequency range 10 Hz to 20 GHz," *Phys. Med. Biol.*, vol. 41, pp. 2251–2269, 1996.
- [28] S. Gabriel, R. W. Lau, and C. Gabriel, "The dielectric properties of biological tissues. 3. Parametric models for the dielectric spectrum of tissues," *Phys. Med. Biol.*, vol. 41, pp. 2271–2293, 1996.
- [29] T. Yamamoto and Y. Yamamoto, "Electrical properties of the epidermal stratum corneum," *Med. Biol. Eng.*, vol. 14, pp. 151–158, 1976.
- [30] P. Rosenfalck, "Intra- and extracellular potential fields of active nerve and muscle fibers. A physico-mathematical analysis of different models," *Acta Physiol. Scand.*, vol. Suppl 321, pp. 1–168, 1969.
- [31] R. Plonsey, "Action potential sources and their volume conductor fields," *Proc. IEEE*, vol. 65, pp. 601–611, 1977.
- [32] C. Gabriel, S. Gabriel, and E. Corthout, "The dielectric properties of biological tissues. 1. Literature survey," *Phys. Med. Biol.*, vol. 41, pp. 2231–2249, 1996.
- [33] N. A. Dimitrova, G. V. Dimitrov, and O. A. Nikitin, "Neither high-pass filtering nor mathematical differentiation of the EMG signals can considerably reduce cross-talk," *J. Electromyogr. Kinesiol.*, vol. 12, pp. 235–246, 2002.



Madeleine M. Lowery (M'00) received the B.E. and Ph.D. degrees from the Department of Electronic and Electrical Engineering, University College Dublin, National University of Ireland, Dublin, Ireland, in 1996 and 2000, respectively.

She is a Research Assistant Professor with the Department of Physical Medicine and Rehabilitation, Northwestern University, Evanston, IL, and a Research Scientist with the Department of Research, Rehabilitation Institute of Chicago. Her research interests include mathematical modeling and analysis of bioelectric signals, and motor control.



Nikolay S. Stoykov (M'00) received the M.S. and Ph.D. degrees in biomedical engineering from the Technical University Ilmenau, Ilmenau, Germany, in 1990 and 1998, respectively. He is a Research Scientist with the Department of Research, Rehabilitation Institute of Chicago, and a Research Assistant Professor with the Department of Physical Medicine and Rehabilitation, Northwestern University, Chicago. His research interests have focused on numerical modeling of bioelectric phenomena.



Julius P. A. Dewald received the B.S. and M.S. degrees in physical therapy and rehabilitation medicine from the Free University of Brussels, Brussels, Belgium, in 1978 and 1980, respectively, and the Ph.D. degree in neurophysiology from Loma Linda University, Loma Linda, CA, in 1992.

He currently holds an Assistant Professorship in the departments of Physical Therapy and Human Movement Sciences, Physical Medicine and Rehabilitation, and Biomedical Engineering at Northwestern University, Evanston, IL. Furthermore, he holds a Senior Clinical Research Scientist position in the Sensory Motor Performance Laboratory at the Rehabilitation Institute of Chicago. His research interests encompass the study of abnormal motor control following injury to the central nervous system using biomechanical, neuroimaging, and system identification techniques.



Todd A. Kuiken (M'99) received the B.S. degree in biomedical engineering from Duke University, Durham, NC, in 1983, the Ph.D. degree in biomedical engineering from Northwestern University, Evanston, IL, in 1989, and the M.D. degree from Northwestern University Medical School, in 1990.

He was the Frankel Research Fellow at the Rehabilitation Institute of Chicago, Chicago, IL, in 1992. He completed a residency in physical medicine and rehabilitation (PM&R) at the Rehabilitation Institute of Chicago in 1995. He was an attending physician at the Rehabilitation Institute of Michigan and an Assistant Professor in the Department of PM&R at Wayne State University Medical School, Detroit, MI, from 1995–1997. He also served as the Director of Orthopedic Rehabilitation. He is currently the Director of Amputee Services at the Rehabilitation Institute of Chicago. He is an Associate Professor in the Department of PM&R and the Electrical and Computer Engineering Department at Northwestern University. He is also the Associate Dean, Feinberg School of Medicine, for Academic Affairs at the Rehabilitation Institute of Chicago. His research interests include prosthetic control systems, using nerve-muscle grafts to obtain additional myoelectric control signal, bioelectromagnetics modeling, prosthetic design, human gait, and care of the amputee.

Dr. Kuiken is a board certified physiatrist.